Biochemical Journal (2016) **473** 4385–4397
DOI: 10.1042/BCJ20160695

PORTLAND PRESS

Research Article

Crystal structure and enantioselectivity of terpene cyclization in SAM-dependent methyltransferase TleD

Feng Yu, Minjun Li, Chunyan Xu, Bo Sun, Huan Zhou, Zhijun Wang, Qin Xu, Muyun Xie, Gang Zuo, Pei Huang, Haojie Guo, Qisheng Wang and Jianhua He

Shanghai Institute of Applied Physics, Chinese Academy of Sciences, 239 Zhang Heng Road, Pudong New District, Shanghai 201203, P.R. China

Correspondence: Feng Yu (yufeng@sinap.ac.cn) or Jianhua He (hejianhua@sinap.ac.cn)

TleD is a SAM (*S*-adenosyl-L-methionine)-dependent methyltransferase and acts as one of the key enzymes in the teleocidin B biosynthesis pathway. Besides methyl transferring, TleD also rearranges the geranyl and indole moieties of the precursor to form a six-membered ring. Moreover, it does not show homologies with any known terpenoid cyclases. In order to elucidate how such a remarkable reaction could be achieved, we determined the complex crystal structures of TleD and the cofactor analogue *S*-adenosyl-L-homocysteine with or without the substrate teleocidin A1. A domain-swapped pattern via an additional N-terminal α-helix is observed in TleD hexamers. Structural comparison and alignment shows that this additional N-terminal α-helix is the common feature of SAM methyltransferase-like cyclases TleD and SpnF. The residue Tyr^{21} anchors the additional N-terminal α-helix to a 'core SAM-MT fold' and is a key residue for catalytic activity. Molecular dynamics simulation results suggest that the dihedral angle C23–C24–C25–C26 of teleocidin A1 is preferred to 60–90° in the TleD and substrate complex structure, which tend to adopt a *Re*-face stereocenter at C25 position after reaction and is according to *in vitro* enzyme reaction experiments. Our results also demonstrate that methyl transfer can be a new chemical strategy for carbocation formation in the terpene cyclization, which is the key initial step.

Introduction

Teleocidin B is a toxin against aquatic organisms produced by *Streptomyces* [1]. It also shows potent tumor-promoting activity via the protein kinase C pathway, and is therefore considered an important natural product in the pharmaceutical field [2]. Teleocidin B is an indolactam-based alkaloid, which possesses a nine-membered ring lactam. (–)-Indolactam V fuses to a six-membered cyclic monoterpenoid with quaternary carbon centers at positions C25 and C19, therefore naturally purified teleocidin B is a mixture of four stereoisomers [3].

In Nature, most terpene cyclizations require a cationic reaction cascade. However, because of the high reactivity of cationic intermediates and transition states, these reactions often need to be carried out inside the enzyme catalytic pockets and are hard to control in solution. In living organisms, the most common terpene cyclization reactions require a pyrophosphate as the leaving group [4]. Thousands of different natural terpene products are generated from just a handful of simple compounds by this reaction mechanism. Other than this canonical terpene cyclization, alternative reaction mechanisms are also found. For example, the reductive terpene cyclization is found in the iridoid biosynthesis pathway [5,6].

Received: 20 July 2016
Revised: 8 September 2016
Accepted: 9 September 2016

Accepted Manuscript online: 9 September 2016
Version of Record published: 25 November 2016

© 2016 The Author(s); published by Portland Press Limited on behalf of the Biochemical Society

Biochemical Journal (2016) **473** 4385–4397
DOI: 10.1042/BCJ20160695

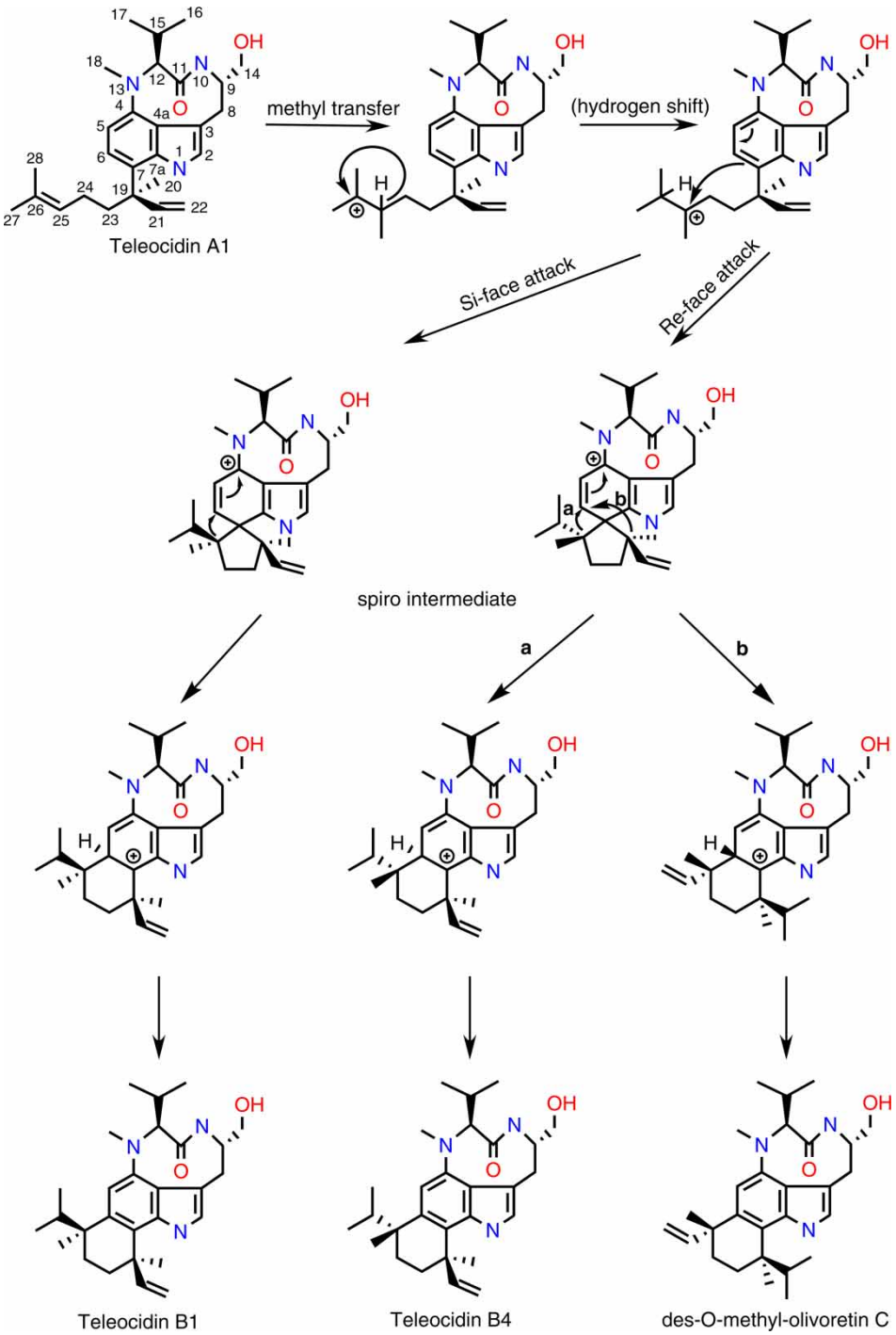

Figure 1. TleD catalyzes teleocidin A to teleocidin B.

TleD is a SAM-MTase, which catalyzes methyl transfer from SAM to the geranyl group of TelA1. After accepting the methyl group, carbocation is formed in the geranyl group of TelA1 and promotes cationic reaction cascade to form cyclic monoterpenoid. There are three products which can be observed. Teleocidin B4 and des-*O*-methyl-olivoretin C are dominant products. In the spiro intermediate, different carbon atom attacks on the C6 atom would form teleocidin B4 or des-*O*-methyl-olivoretin C respectively. Teleocidin B1 also can be formed through *Si*-face attack after hydrogen shift, but it requires overcoming extra potential barrier of conformational change. In our complex crystal structure, we did not find reasonable residues which can accept the hydrogen atom at the C6 position in the final reaction step. We therefore speculate that this hydrogen atom is eliminated through an E1-like reaction. The electron transfer pathway movements in the reaction are shown as arrows.

© 2016 The Author(s); published by Portland Press Limited on behalf of the Biochemical Society

Biochemical Journal (2016) **473** 4385–4397
DOI: 10.1042/BCJ20160695

The enzyme TleD catalyzes TelA1 (teleocidin A1) to teleocidin B1, teleocidin B4 and des-*O*-methyl-olivoretin C, which undergoes a monoterpenoid cyclization step [7] (Figure 1). Teleocidin B4 and des-*O*-methyl-olivoretin C are dominant reaction products. Unexpectedly, TleD does not resemble a terpene cyclase, but rather a class I SAM-MTase [SAM (*S*-adenosyl-L-methionine)-dependent MTase (methyltransferase)]. TleD is the first MTase-like protein which can catalyze terpene cyclization [7]. It is therefore believed that exploring the structure and reaction mechanism of TleD would expand our understanding of methyl transfer and terpene cyclization reactions. Despite a full understanding of TleD catalysis process not having emerged, it is proposed that the cationic reaction cascade is triggered after TelA1 accepts a methyl group from SAM, which is consistent with the SAM-MTase mechanism.

To clarify the TleD catalytic mechanism, we determined the crystal structure of TleD and cofactor analogue SAH (*S*-adenosyl-L-homocysteine) complex with or without the substrate TelA1. Although the overall folds of SAM-MTases are highly conserved, the precise position of various structure elements differs substantially, especially in the regions controlling substrate specificity. Molecular dynamics simulation results suggest that the dihedral angle C23–C24–C25–C26 of TelA1 is preferred to 60–90° in the TleD–SAM–TelA1 complex structure, which tends to adopt a *Re*-face stereocenter at the C25 position after reaction and is according to enzyme reaction experiments. Site-directed mutagenesis, LC–MS experiments, structural comparison and alignment results indicate that an additional N-terminal α-helix, which is the common feature of TleD and another MTase-like cyclase SpnF, possibly facilitates the 'core SAM-MT fold' [8] to generate an enclosed active site and promotes substrates to adopt the proper conformation for the reaction.

Experimental

Protein expression and purification

The total synthesis of TleD cDNA was based on GenBank® AB937726, and codon usage was optimized for the *Escherichia coli* expression system. The optimized TleD cDNA sequence was submitted as Supplementary Online Data. The full-length TleD cDNA sequence was constructed into pET-22b vector using NdeI/XhoI enzyme sites (pET22b-TleD), which produced a C-terminal His-tagged protein. Wild-type TleD protein was auto-inducted in *E. coli* BL21(DE3) cells using LB broth with 0.2% D-lactose and 0.05% D-glucose [9]. After 12 h of induction at 20°C, bacteria were centrifuged at 7000 ***g*** for 10 min. The resulting cell pellet was resuspended in buffer A (20 mM Tris/HCl, pH 8.0, 300 mM NaCl and 5% glycerol), and then lysed by passing through a microfluidizer (1250–1500 bar; 1 bar=100 kPa) twice. The lysate was centrifuged at 30 000 ***g*** for 30 min. The supernatant was loaded into a 5 ml Ni-IDA (Ni^{2+}-iminodiacetic acid) column (GE Healthcare) which had been equilibrated with buffer A, and then eluted by buffer B (20 mM Tris/HCl, pH 8.0, 300 mM NaCl, 300 mM imidazole and 5% glycerol). After dilution with buffer C (20 mM Tris/HCl, pH 8.0, and 5% glycerol), the sample was loaded on to a HiTrap Q FF column and eluted by a linear gradient. Finally, TleD was loaded on to a Superdex 200 16/60 column which was equilibrated with buffer D (25 mM Tris/HCl, pH 8.0, 150 mM NaCl and 5% glycerol). The target protein was concentrated to 15 mg/ml by a 30 kDa molecular-mass cut-off Amicon Ultra filter (Millipore). Aliquots were snap-frozen in liquid nitrogen and stored at −80°C until they were used for crystallization.

Site-directed mutagenesis

The Y21F (TleD-Y21F), Y21L (TleD-Y21L), Y28F (TleD-Y28F), Y28L (TleD-Y28L), Y200F (TleD-Y200F) and Y200L (TleD-Y200L) mutants were produced by applying mutagenic PCR to the pET22b-TleD plasmid according to the QuikChange® (Agilent) protocol. All mutant plasmids were sequenced to confirm the desired mutations. Plasmids containing the confirmed TleD mutations were then transformed into *E. coli* BL21(DE3) cells, and the corresponding overexpressed recombinant mutant proteins were purified as described for the wild-type enzyme.

Protein crystallization

Before crystallization, fresh SAM or SAH was added to protein solution to 2 mM final concentration. Crystals of TleD were grown using the hanging-drop vapour-diffusion method at 18°C. We did not observe any TleD crystals under the crystallization conditions used without SAM or SAH. Finally, high-quality TleD–SAH complex crystals were obtained after protein solution mixed with equal volumes of the reservoir solution containing 100 mM Tris/HCl, pH 8.0, 18% PEG400, 14% PEG3350, 100 mM $MgCl_2$ and 2 mM TCEP [Tris (2-carboxyethyl)phosphine]. TleD–SAH–TelA1 complex crystals were obtained under the same crystallization

© 2016 The Author(s); published by Portland Press Limited on behalf of the Biochemical Society

Biochemical Journal (2016) **473** 4385–4397
DOI: 10.1042/BCJ20160695

Table 1. Data collection and refinement statistics

Values in parentheses are for the highest resolution shell. $R=\Sigma_{hkl}|F_{obs}-F_{calc}|/\Sigma_{hkl}F_{obs}$. R_{free}, calculated the same as R_{work}, but from a test set containing 5% of data excluded from the refinement calculation.

	Substrate-free TleD (PDB code 5GM1)	Substrate-bound TleD (PDB code 5GM2)
Data collection		
Space group	*C*2	*C*2
a (Å)	259.6	257.5
b (Å)	152.9	152.8
c (Å)	154.8	154.2
β (°)	93.3	93.1
Resolution (Å)	154.53–2.50 (2.64–2.50)	153.95–2.80 (2.95–2.80)
R_{merge} (%)	8.0 (49.1)	7.2 (48.4)
$CC_{1/2}$	0.998 (0.835)	0.999 (0.846)
$<I/\sigma I>$	14.5 (3.1)	16.5 (3.3)
Completeness (%)	99.0 (96.3)	99.8 (100.0)
Multiplicity	5.4 (5.5)	4.7 (4.8)
Refinement		
Number of reflections	205 755	146 088
R_{work}/R_{free} (%)	20.75/24.81	20.66/24.87
Number of atoms		
Protein	38 966	37 995
Ligand	520	1044
Water	696	166
RMSD		
Bond lengths (Å)	0.003	0.003
Bond angles (°)	0.592	0.713
Ramachandran plot (%)		
Favored	97.57	95.20
Allowed	1.99	3.55
Outliers	0.44	1.25

conditions using the co-crystallization method. TelA1 was purchased from BioAustralis (catalog number BIA-T1429) and was added to a molar concentration equal with protein. Higher TelA1 concentrations would lead to precipitation, because TelA1 is nearly insoluble in water. Crystals were cryoprotected with the cryoprotectant (The cryoprotectant contains 100 mM Tris/HCl 8.0, 21% PEG400, 17% PEG3350, 50 mM $MgCl_2$, 20% glycerol) before freezing in liquid nitrogen.

Data collection and structure determination

X-ray diffraction data were collected at beamline BL17U1 of the Shanghai Synchrotron Radiation Facility [10]. Data were integrated by autoPROC [11] and XDS [12], then merged and scaled by AIMLESS [13]. The structure was solved by molecular replacement using Phaser with SpnF [14] from *Saccharopolyspora spinose* (PDB code 4PNE) as the search model. After molecular replacement, maximum likelihood-based refinement of the atomic positions and temperature factors were performed with Phenix [15]. The atomic model was fitted using the program Coot [16]. The stereochemical quality of the final model was assessed using MolProbity [17]. Crystallographic statistics for the final model are shown in Table 1. Figures were prepared using PyMOL (DeLano Scientific; http://www.pymol.org).

© 2016 The Author(s); published by Portland Press Limited on behalf of the Biochemical Society

Biochemical Journal (2016) **473** 4385–4397
DOI: 10.1042/BCJ20160695

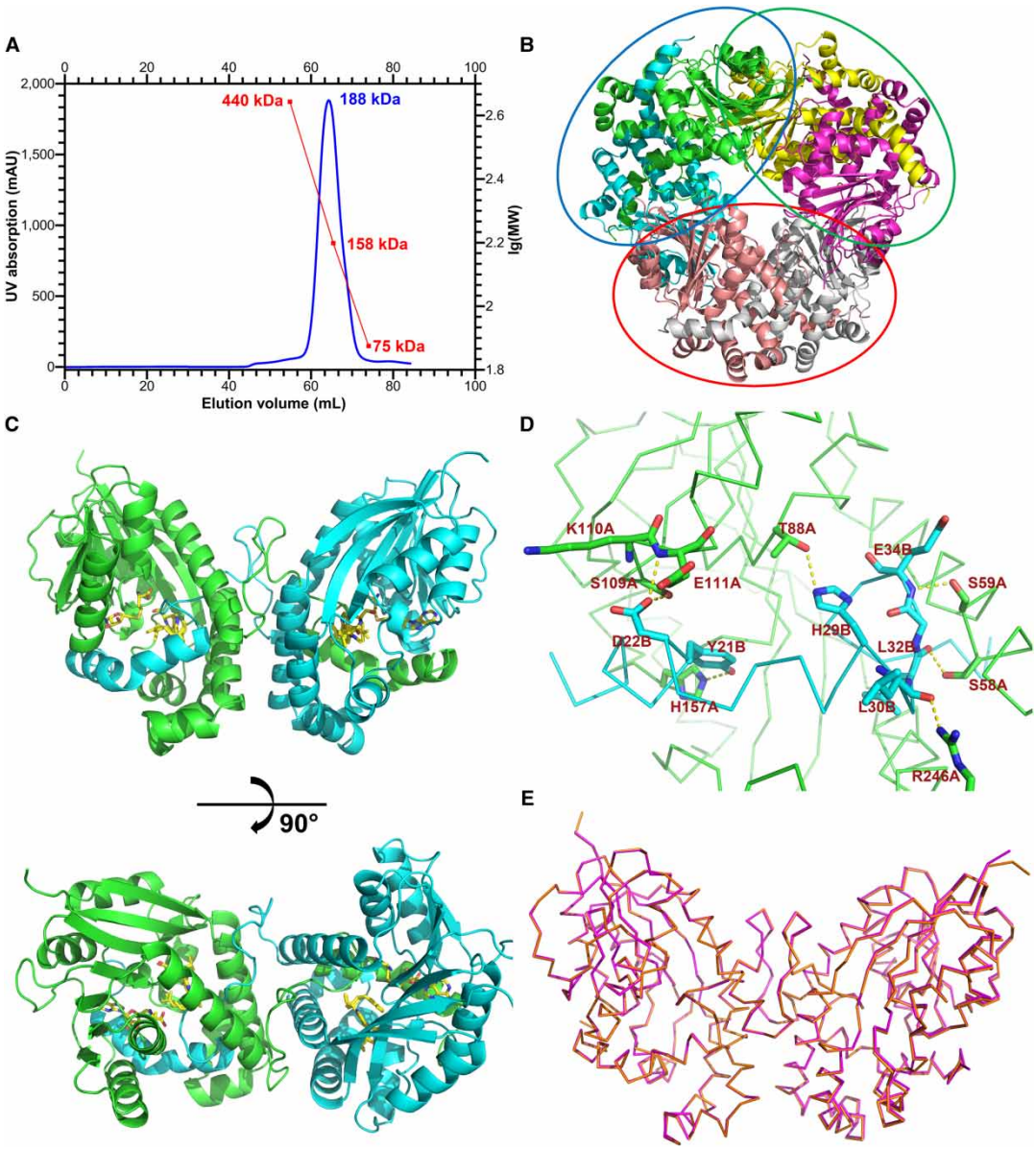

Figure 2. Structure of TleD.

(**A**) Characterization of TleD in solution. The molecular mass of TleD monomer is ~31.7 kDa. Gel filtration results show that the apparent molecular mass of the purified wild-type TleD is ~188 kDa, which indicates that TleD exists as a hexamer in solution. The red line is the fitted standard curve. (**B**) Overall structure of the TleD hexamer. Each chain is drawn using a different color. The TleD hexamer can be divided into three groups, marked by three ellipses. Each group contains two domain-swapped TleD molecules. (**C**) Horizontal and vertical views of domain-swapped pattern in TleD. An α-helix of N-terminal inserts into the partner molecule to produce the integral active site. TelA1 and SAH are drawn as sticks with yellow carbon atoms. (**D**) Polar contacts between the N-terminal α-helix of dimerization partner and the 'core SAM-MT fold'. It is noted that the hydrogen bond between Tyr^{21B} and His^{157A} is important for the local protein fold. Chain A is drawn with green carbon atoms, and chain B is drawn with cyan carbon atoms. The interacting residues are drawn as sticks. (**E**) Superimposition of substrate-bound and substrate-free TleD. The substrate-bound and substrate-free TleD are colored magenta and orange respectively. The RMSD of Cα atoms between the substrate-free and the substrate-bound molecules is only 0.21 Å.

© 2016 The Author(s); published by Portland Press Limited on behalf of the Biochemical Society

Biochemical Journal (2016) 473 4385–4397
DOI: 10.1042/BCJ20160695

Molecular dynamics simulation

Before simulation, SAH was mutated to SAM and hydrogen atoms were added to the TleD–SAM–TelA1 complex (54–290 of chain A, 10–41 of chain B, SAM and TelA1) by using PDB2PQR [18] and PROPKA 3.1 [19]. Two complexes with different geranyl conformations of TelA1 were prepared and simulated separately. Partial atomic charges of SAM and TelA1 were calculated by AmberTools 15 [20] and Gamess-US [21] using the RESP method [22]. Molecular mechanics parameters for TleD were taken from the Amber14SB force field. A water box with TIP3P water and counterions was also built. The final model of the complex consisted of 44 883 atoms, including the TleD protein, SAM, TelA1, 13 542 water molecules, and 11 Na^+ ions to neutralize the whole system. After geometry optimization and equilibrium, 10 ns molecular dynamics simulations at 300 K were performed on each TleD–SAM– TelA1 complex. Distance and dihedral information were analyzed using CPPTRAJ [23].

Enzymatic reactions and LC–MS analysis

Concentrations of 20 μM TleD, 150 μM AdoMet and 100 μM TelA1 were incubated in a total volume of 50 μl of Tris buffer (50 mM Tris/HCl, pH8.5, 100 mM NaCl and 2 mM $MgCl_2$). The reaction mixture was incubated at room temperature for 300 min. After that, the solution was extracted with ethyl acetate. The organic layer was evaporated to dryness and the supernatant was discarded. The residual material was resuspended using DMSO and filtered using 0.22 μm centrifugal filter tubes (Millipore). Then, the final samples were analyzed using LC–MS (Waters 2695 HPLC and Waters ZQ2000 mass detector).

Circular dichroism spectra analysis

To confirm that the Y21F mutation did not affect the global protein fold, wild-type TleD and TleD-Y21F were analyzed by CD spectroscopy (Chirascan, Applied PhotoPhysics). CD spectra were recorded from 180 to 280 nm at 1 nm intervals by using a 0.1-mm-pathlength quartz cell and 0.7 mg/ml protein concentration.

Results

Overall structure

Gel filtration results show that the purified TleD exists as hexamers in solution (Figure 2A). We co-crystallized TleD and its cofactor analogue SAH complex with and without substrate TelA1. Both crystals belong to space group *C*2, and the resolutions of substrate-free and substrate-bound crystal structures are at 2.50 and 2.80 Å (1 Å=0.1 nm) respectively. Detailed crystallographic statistic data are shown in Table 1.

Three TleD hexamers are found in the asymmetric unit related by non-crystallographic symmetry. Surprisingly, a domain-swapped pattern is observed in TleD hexamers (Figure 2B,C), which is rarely found in SAM-MTases. Each TleD hexamer can be divided into three groups, and each group contains two domain-swapped TleD molecules. The TleD molecule possesses a typical class I SAM-MTase fold with an additional α-helix in the N-terminus. This additional α-helix inserts into the 'core SAM-MT fold' of its partner molecule mutually and produces an integral active site. The polar contacts between the N-terminal α-helix of the partner molecule and the 'core SAM-MT fold' are shown in the Figure 2D. The RMSD of Cα atoms between the substrate-free molecule and the substrate-bound molecule is only 0.21 Å. The superimposition of these two crystal structures shows that there is not significant conformational change after substrate TelA1 binding (Figure 2E).

The structure of the active site

The electron density of the cofactor SAH (Figure 3A) is well defined in the TleD complex structure. The SAM/SAH-binding site is located in the Rossmann fold which is conserved in all of the class I SAM-MTases. SAH is bound through an extensive hydrogen-bond network and van der Waals interactions, and is partially exposed to solvent. The substrate TelA1 is buried in a hydrophobic cavity, which is defined by Tyr^{21}, Tyr^{28}, Leu^{32}, Val^{36}, Leu^{37}, Cys^{38}, Glu^{153}, His^{157}, Leu^{180}, Glu^{181}, Ser^{182}, Phe^{196}, Tyr^{200}, Leu^{232}, Met^{236}, Thr^{235}, Leu^{273} and Phe^{279} (Figure 3B). On the basis of this TleD complex crystal structure, it is found that the active pocket is compact and just accommodates TelA1. No water molecule is observed inside the active pocket. Two hydrogen bonds are found between TelA1 and the surrounding resides (Glu^{153} and Glu^{181}), which might determine the substrate orientation.

© 2016 The Author(s); published by Portland Press Limited on behalf of the Biochemical Society

Biochemical Journal (2016) **473** 4385–4397
DOI: 10.1042/BCJ20160695

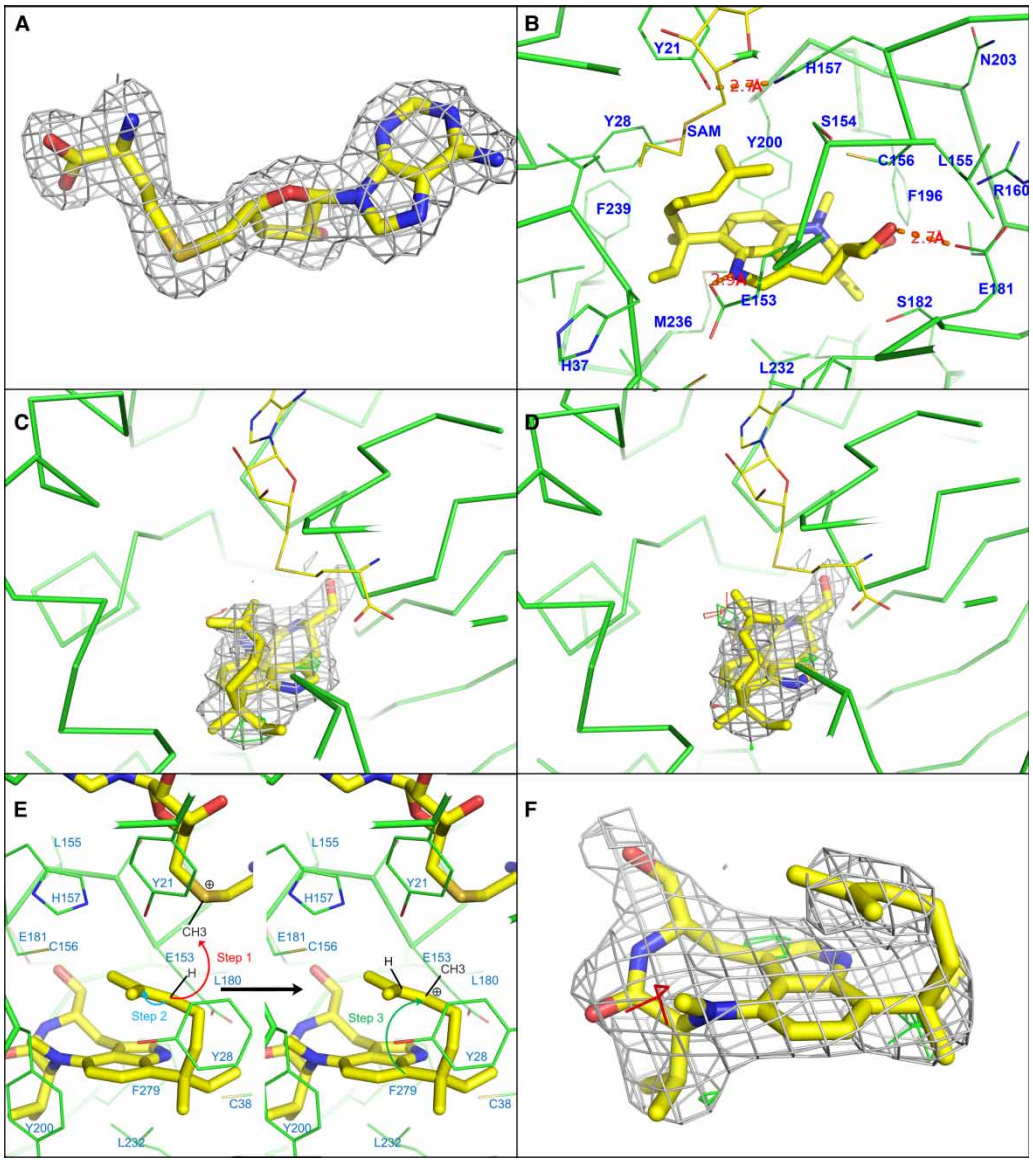

Figure 3. The structure of the TleD active site.

(**A**) Electron density map of SAH. (**B**) Structure of TleD active site. The backbone is drawn as a ribbon with green Cα atoms. The side chains, which surround TelA1 within 5 Å, are drawn as lines with green carbon atoms. TelA1 and SAH are drawn with yellow carbon atoms. Hydrogen bonds are drawn as broken lines with bond lengths labeled in red. (**C** and **D**) Two possible geranyl conformations. Dihedral angles C23–C24–C25–C26 were approximately 58° and −129° in (**C** and **D**) respectively. (**E**) Reaction schemes. SAM carries an activated methyl group, which is electron-deficient, and is well suited for methyl transfer through an S_N2 reaction mechanism. The double bond of terpene, as an electron donor, also is apt to accept a positively charged methyl group from SAM. After C25 accepting a methyl group, the original double bond between C25 and C26 becomes a single bond and C26 obtains positive charges (step 1). *In vitro* enzyme activity analysis had proved that a hydrogen shift would happen between C25 and C26 after the methyl transfer and lead to electrons transferring from C25 to C26 (step 2). After that, C25 carries positive charges, whereas C7, which is close to C25 in the 3D structure, is electron-rich because of the aromatic ring. C7 would therefore tend to attack C25 to form a spiro intermediate (step 3). In the present study, we show the dihedral angle C23–C24–C25–C26 should be close to 58°. With this binding pose, C7 must tend to *Re*-face attack C25, hence the spiro intermediate will adopt a *Re*-face stereocenter at the C25 position and form teleocidin B4 and des-*O*-methyl-olivoretin C. The side chains surrounding TelA1 within 5 Å are drawn as lines with green carbon atoms. The electron transfer pathway movements in the reaction are shown as arrows. (**F**) The electron density map of TelA1 with the former geranyl conformation. $2F_o–F_c$ maps were contoured at 1σ and $F_o–F_c$ maps are contoured at ± 3 σ.

© 2016 The Author(s); published by Portland Press Limited on behalf of the Biochemical Society

PORTLAND PRESS

Biochemical Journal (2016) **473** 4385–4397
DOI: 10.1042/BCJ20160695

Geranyl conformations possibly determine the chirality of products

Because of low resolution and/or structural flexibility, the electron density hints at two possible geranyl conformations (Figure 3C,D) which are rotamers caused by the flipping of the dihedral angle C23–C24–C25–C26. They are ∼58° and −129° in those two conformations respectively. It is hard to identify the correct one between both conformations through electron density or *R*-factors. Attempts to obtain higher-resolution complex structures also failed.

It is well known that teleocidin B has four stereoisomers, among which teleocidin B1 and B4 are distinguished from each other through chiral atom C25. A possible reaction mechanism of TleD had been proposed by Awakawa et al. [7]. It is proposed that a cationic reaction cascade is triggered after TelA1 accepting a methyl group from SAM (Figure 3E). After C25 accepting a methyl group, the original double bond between C25 and C26 becomes a single bond and C26 becomes a tertiary carbocation. *In vitro* enzyme activity analysis has

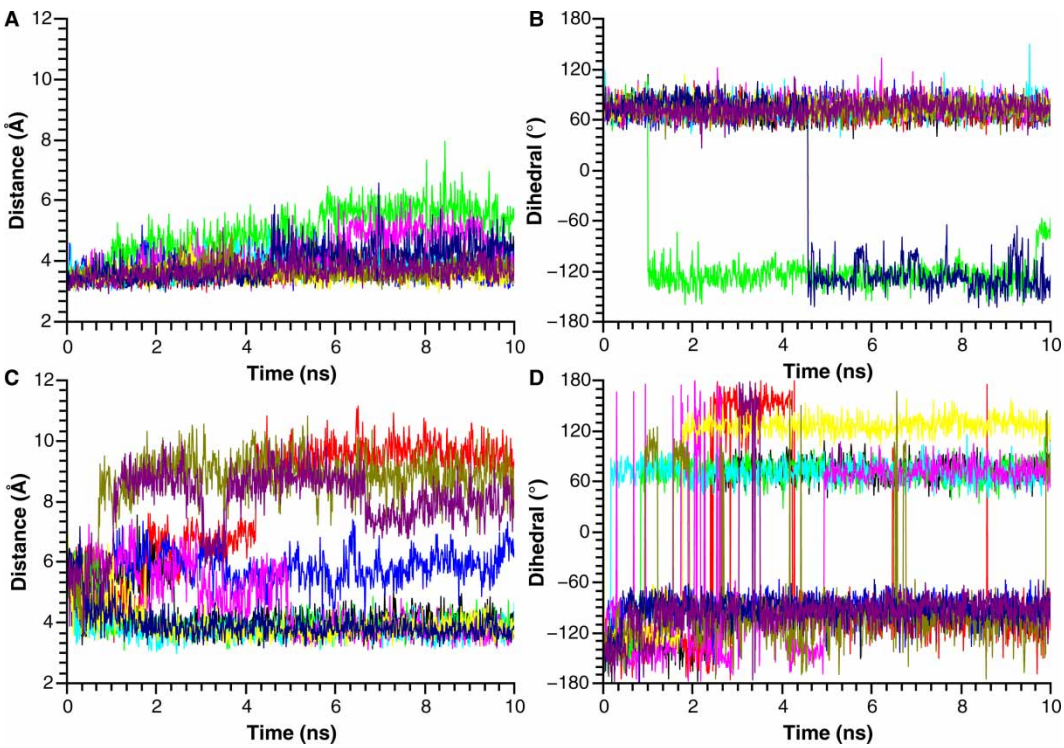

Figure 4. Analysis of molecular dynamics trajectories.

(**A** and **B**) Trajectories of the distances between Cε of SAM's methionine moiety and C25 of TelA1, and the dihedral angle C23–C24–C25–C26 with its initial value set to 58°. The methyl transfer reaction requires a linear alignment of the acceptor substrate, methyl group ($C\varepsilon^{SAM}$), and the donor ($S\delta^{SAM}$), in which methyl group and its acceptor also should be close enough in space. Seven of ten trajectories hold the dihedral angle C23–C24–C25–C26 at ∼60–90°, the distance between $C\varepsilon^{SAM}$ and $C25^{TelA1}$ was also maintained at less than 4 Å. In the other three trajectories (green, navy and pink), the distance between $C\varepsilon^{SAM}$ and $C25^{TelA1}$ increased obviously, and two (green and navy) of them changed dihedral angle to −120°. (**C** and **D**) Trajectories of the distances between Cε of SAM's methionine moiety and C25 of TelA1 and the dihedral angle C23–C24–C25–C26 with its initial value set to −129°. None of the trajectories could hold the dihedral angle at approximately −120° and maintained a reasonable distance between the methyl group and its acceptor simultaneously. Four (blue, purple, red and dark yellow) out of ten trajectories maintain dihedral angle at approximately −90°. However, the distances between $C\varepsilon^{SAM}$ and $C25^{TelA1}$ increased to ∼6–10 Å, which are too large compared with common distances for methyl transfer. One trajectory (pink) changed the dihedral angle to ∼60° after 5 ns of simulation and one trajectory (yellow) changed the dihedral angle to ∼120° after 2 ns of simulation. The remaining four trajectories changed the dihedral angle to 60° after less than 1 ns of simulation. These results indicate that the dihedral angle C23–C24–C25–C26 close to 60–90° was the preferred geranyl conformation in the TleD–SAM–TelA1 complex. All distances and dihedral angles were recorded for 10 ns at 10 ps intervals. The same color represents the same trajectory in (**A**) and (**B**) or (**C**) and (**D**) respectively.

© 2016 The Author(s); published by Portland Press Limited on behalf of the Biochemical Society

Biochemical Journal (2016) **473** 4385–4397
DOI: 10.1042/BCJ20160695

proved a hydrogen shift would happen between C25 and C26 after the methyl transfer and lead to positive charges transferring from C26 to C25. After that, a spiro intermediate would be further formed through the C25 bond on C7. In the spiro-ring formation process, the facial selectivity of the nucleophilic attack to the C25 cationic intermediate could determine the C25 atom chirality of the product. Therefore, it should be noted that the different geranyl conformation tends to generate the different enantiomer with chiral atom at the C25 position. When the dihedral angle is close to 58°, the product tends to adopt an *Re*-face stereocenter at the C25 position after reaction (Figure 3C), namely teleocidin B4 and des-*O*-methyl-olivoretin C. Correspondingly, after dihedral angle flipping, teleocidin B1 tends to be generated, which adopts an *Si*-face stereocenter at the C25 position (Figure 3D). Since teleocidin B4 and des-*O*-methyl-olivoretin C are the dominant reaction products, the former conformation, in which the dihedral angle is close to 58°, should be correct (or dominant at least). The distances between Sδ of SAH and C25 of TelA1 in the former conformation is 4.52 Å, which is the common distance between the acceptor and Sδ atom in MTases. The electron density of TelA1 with the former conformation is shown in Figure 3F.

Molecular dynamics simulation

Because the geranyl conformation of substrate was vital to the chirality of products and hard to identify in the complex crystal structure, to confirm further the geranyl conformation, we performed molecular dynamics simulations with different conformations to test the stability of geranyl conformations. Each geranyl conformation was simulated for ten 10-ns trajectories. The distance between Cε of SAM's methionine moiety and C25 of TelA1 and the dihedral angle C23–C24–C25–C26 were recorded at 10 ps intervals. The detailed trajectories are shown in Figure 4. The methyl transfer reaction requires a linear alignment of the acceptor substrate, methyl group ($C\varepsilon^{SAM}$), and the sulfur atom ($S\delta^{SAM}$), in which the methyl group and its acceptor also should be close enough in space. When the former conformation (with the dihedral angle close to 58°) was used as the initial conformation, seven of ten trajectories hold the dihedral angle C23–C24–C25–C26 at ∼60–90°, the distance between $C\varepsilon^{SAM}$ and $C25^{TelA1}$ was also maintained at less than 4 Å. In the other three trajectories, the distance between Cε of SAM and C25 of TelA1 increased obviously, and two trajectories changed the dihedral angle to approximately −120°. In contrast, when the latter conformation (with the dihedral angle close to −129°) was used as the initial conformation, none of the trajectories could hold the dihedral angle at approximately −120°

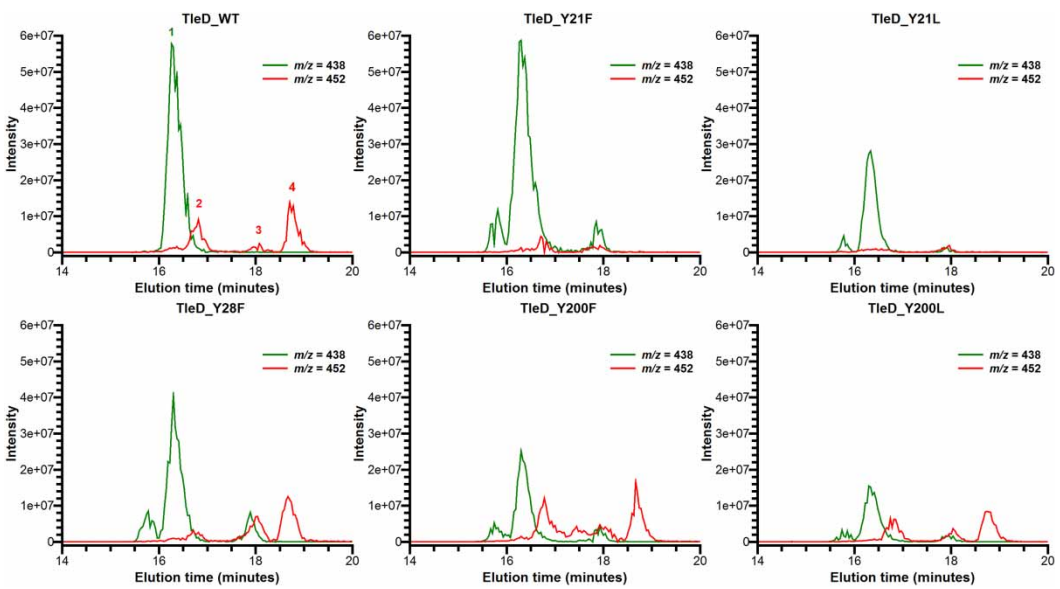

Figure 5. Enzyme activity assay.

Enzyme reaction products were analyzed using LC–MS. The *m/z* of the reactant is 438 (green lines), and the *m/z* of the product is 452 (red lines). After mutating Tyr^{21} to phenylalanine or leucine, the amount of protein expression was drastically reduced compared with that of native protein (TleD-WT). Peak 1, TelA1; peak 2, des-*O*-methyl-olivoretin C; peak 3, teleocidin B1; peak 4, teleocidin B4.

© 2016 The Author(s); published by Portland Press Limited on behalf of the Biochemical Society

Biochemical Journal (2016) 473 4385–4397
DOI: 10.1042/BCJ20160695

and maintained a reasonable distance between methyl group and its acceptor at the same time. Four of ten trajectories maintained the dihedral angle at approximately −90°, but distances between $C\varepsilon^{SAM}$ and $C25^{TelA1}$ changed to ∼6–10 Å, which are too large compared with the common distances in the MTases. One trajectory (pink) changed the dihedral angle to ∼60° after 5 ns of simulation and one trajectory changed the dihedral angle to ∼120° after 2 ns of simulation. The remaining four trajectories changed the dihedral angle to ∼60–90° after less than 1 ns of simulation. These results indicate that the dihedral angle C23–C24–C25–C26 close to 60–90° was the preferred geranyl conformation in the TleD–SAM–TelA1 complex and confirmed further that the former conformation was the correct one in the TleD–SAM–TelA1 complex crystal structure.

Tyr^{21}, a key residue for catalysis activity, anchors the additional N-terminal α-helix to the 'core SAM-MT fold'

Glu^{153} and Glu^{181}, which interact with substrate through hydrogen bonds, were residues known to play the role in substrate binding. To inspect other key residues for catalysis, we selected three residues (Tyr^{21}, Tyr^{28} and Tyr^{200}, each mutated to both leucine and phenylalanine) which are close to the substrate reaction region for mutagenesis. Except that the purification of Y28L was unsuccessful, Y28F, Y200F and Y200L mutants displayed similar enzymatic activity to that of the wild-type TleD. However, the enzymatic activity of Y21F and Y21L mutants decreased dramatically (Figure 5), although CD spectra confirmed that Y21F did not change the global protein fold (Figure 6). As shown in the TleD structure, a hydrogen bond between Tyr21 and the His157 side chain was one of the vital polar contacts to firm mutual position of the additional N-terminal α-helix and the 'core SAM-MT fold'. The TleD-Y21F mutagenesis experiments implied that the hydrogen bond between Tyr^{21} and His^{157} played the most important role in maintaining the local protein fold which was important for enzyme activity.

Discussion

Structural homology comparison with SpnF

In the present study, we solved the first SAM-MTase crystal structure which can catalyze terpene cyclization. At present, hundreds of class I SAM-MTase structures have been deposited in the PDB. These enzymes show no or very low overall sequence identity with each other, but share a common 'core SAM-MT fold'. Many members also contain additional domains outside the 'core SAM-MT fold' that play a role in substrate recognition or alternative functions.

In the PDB, MTase-like enzyme SpnF [14], which is one of the key enzymes in the biosynthesis pathway of spinosyn A, is the closest homologous structure with TleD. Surprisingly, SpnF possesses a 'core SAM-MT fold'

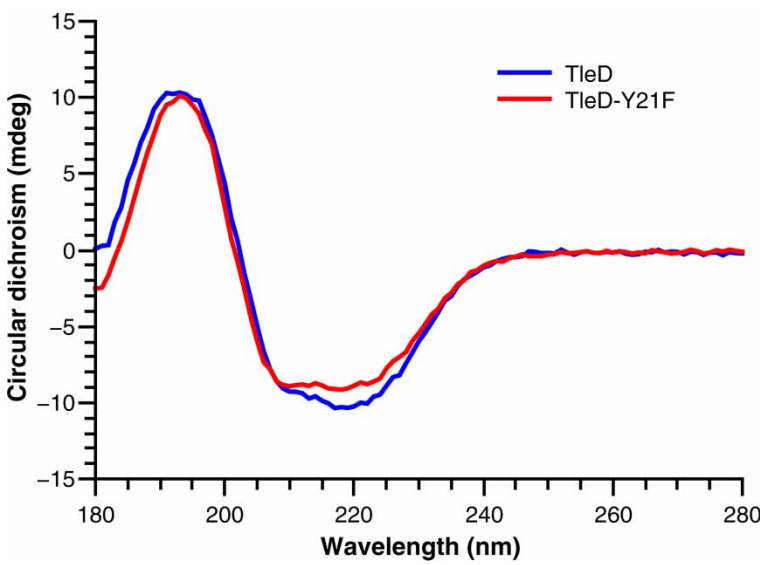

Figure 6. CD spectra of wild-type TleD and TleD-Y21F.

There were only slight differences between the two CD spectra. This implies that TleD-Y21F mutant and wild-type TleD had the same global fold. The differences may be caused by local fold changes in the TleD-Y21F mutant.

© 2016 The Author(s); published by Portland Press Limited on behalf of the Biochemical Society

Biochemical Journal (2016) **473** 4385–4397
DOI: 10.1042/BCJ20160695

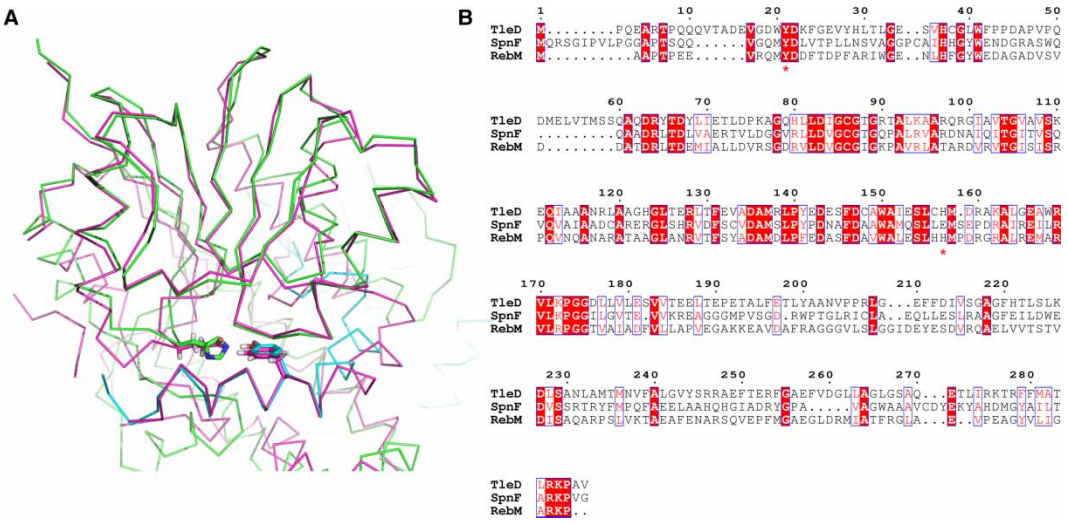

Figure 7. Structure and sequence comparisons between TleD and SpnF.

(**A**) The superimposing of TleD and SpnF. Chain A of TleD is colored green, chain B is colored cyan, and SpnF is colored magenta. The 'core SAM-MT fold' of chain A and the N-terminal α-helix of chain B align with SpnF excellently. Tyr^{21TleD}, $His^{157TleD}$, Tyr^{23SpnF} and $Glu^{152SpnF}$ are drawn as sticks. (**B**) Sequence comparison between TleD, SpnF and rebeccamycin 4′-*O*-methyltransferase, RebM. Conserved residues which anchor the N-terminal α-helix to the 'core SAM-MT fold' in TleD and SpnF are indicated by a red star. Although RebM is highly homologous with TleD and SpnF, it does not possess cyclase activity [28] and the N-terminal region (residues 1–22) is lacking in the crystal structure (PDB code 3BUS).

and binds SAH, but it performs a [4 + 2] cycloaddition on substrates through a Diels–Alder mechanism and does not have any known MTase activity. The function of SAM/SAH in SpnF is unknown. A reaction mechanism was recently proposed by QM/MM (quantum mechanics/molecular mechanics) simulation [24]. It is interesting to note that SpnF also contains an additional N-terminal α-helix which anchors to the 'core SAM-MT fold' through the hydrogen bond between Tyr^{23SpnF} and $Glu^{152SpnF}$ and produces an integrated active site. It indicates that this hydrogen bond is conserved in TleD and SpnF (Figure 7). Both enzymes catalyzing terpene cyclization and [4 + 2] cycloaddition require substrates to adopt the proper conformations before overcoming the reaction potential barrier. Therefore, we propose that the additional N-terminal α-helix facilitates the 'core SAM-MT fold' to produce a relatively sealed environment and promote substrates to adopt proper conformations.

Carbocation, which is necessary for promoting terpene cyclization, could be formed by methyl transferring from SAM

In the canonical terpenoid cyclase-catalyzed reaction, the cyclase reaction is initiated by the formation of a highly reactive carbocation. The most common chemical strategy is using a pyrophosphate (PP_i) as the leaving group [4]. In some other terpenoid cyclases, protonation of an epoxide ring [25] or a carbon–carbon double bond [26] are also found. In the present study, we demonstrate a new chemical strategy of carbocation formation for promoting terpene cyclization. Carbocation, which is necessary for promoting terpene cyclization, could be formed by methyl transfer from SAM. SAM carries an activated methyl group, which is electron-deficient, and is well suited for methyl transfer through an S_N2 reaction mechanism. The double bond of terpene, which is electron-rich, also is apt to accept a methyl group from SAM. Therefore, after the methyl transfer reaction, carbocation is formed in the geranyl of TelA1, which promotes a cationic reaction cascade to form a cyclic monoterpenoid.

The hydrophobic active pocket is suited for methyl transfer reaction and terpene cyclization

Proximity and desolvation effects are common methyl transfer reaction mechanisms [27] and can be observed in this structure. The architecture and chemical environment of the enzyme active pocket ensure that the

© 2016 The Author(s); published by Portland Press Limited on behalf of the Biochemical Society

Biochemical Journal (2016) **473** 4385–4397
DOI: 10.1042/BCJ20160695

acceptor directly attacks the S-methyl group of SAM (methyl donor), and water molecules are excluded from the donor/acceptor interface. Besides methyl transfer reactions, terpene cyclization reactions also require a hydrophobic environment due to the high reactivity of carbocation intermediates and transition states. TelA1 is almost insoluble in water. However, TleD provides a hydrophobic environment, which binds TelA1 effectively in our experiments. Because of the compact active pocket, no water molecules could enter the active pocket in the complex structure. Even in the molecular dynamics equilibrium structure, no water molecule was observed in the active pocket. In our complex crystal structure, we did not find reasonable residues which can accept the hydrogen atom at the C6 position in the final reaction step. Therefore, we speculate this hydrogen atom is eliminated through an E1-like reaction.

Abbreviations

MTase, methyltransferase; SAH, *S*-adenosyl-L-homocysteine; SAM, *S*-adenosyl-L-methionine; SAM-MTase, SAM-dependent MTase; TelA1, teleocidin A1.

Author Contribution

F.Y., M.L., C.X., B.S. and J.H. designed the study and wrote the paper. F.Y., H.Z., Q.W. and P.H. purified and crystallized the protein and determined its X-ray structure. F.Y., Q.X. and M.X. characterized enzyme activity *in vitro*. H.G. and G.Z. designed and constructed vectors for the expression of mutant proteins. F.Y., B.S. and Z.W. performed molecular dynamics simulations. All authors analyzed the results and approved the final version of the paper.

Funding

This work was supported by the National Natural Science Foundation of China [grant numbers 31570740 and 81330076] and Youth Innovation Promotion Association of Chinese Academy of Sciences [grant number 2015213].

Acknowledgements

The structure co-ordinates and structure factors have been deposited in the PDB under codes 5GM1 and 5GM2.

Competing Interests

The Authors declare that there are no competing interests associated with the manuscript.

References

1 Takashima, M. and Sakai, H. (1960) A new toxic substance, teleocidin, produced by *Streptomyces*. *Bull. Agr. Chem. Soc. Jpn.* **24**, 647–655
2 Fujiki, H., Mori, M., Nakayasu, M., Terada, M., Sugimura, T. and Moore, R.E. (1981) Indole alkaloids: dihydroteleocidin-B, teleocidin, and lyngbyatoxin-a as members of a New class of tumor promoters. *Proc. Natl. Acad. Sci. U.S.A.* **78**, 3872–3876
3 Hitotsuyanagi, Y., Fujiki, H., Suganuma, M., Aimi, N., Sakai, S., Endo, Y. et al. (1984) Isolation and structure elucidation of teleocidin B-1, B-2, B-3, and B-4. *Chem. Pharm. Bull.* **32**, 4233–4236
4 Christianson, D.W. (2006) Structural biology and chemistry of the terpenoid cyclases. *Chem. Rev.* **106**, 3412–3442
5 Geu-Flores, F., Sherden, N.H., Courdavault, V., Burlat, V., Glenn, W.S., Wu, C. et al. (2012) An alternative route to cyclic terpenes by reductive cyclization in iridoid biosynthesis. *Nature* **492**, 138–142
6 Kries, H., Caputi, L., Stevenson, C.E.M., Kamileen, M.O., Sherden, N.H., Geu-Flores, F. et al. (2016) Structural determinants of reductive terpene cyclization in iridoid biosynthesis. *Nat. Chem. Biol.* **12**, 6–8
7 Awakawa, T., Zhang, L.H., Wakimoto, T., Hoshino, S., Mori, T., Ito, T. et al. (2014) A methyltransferase initiates terpene cyclization in teleocidin B biosynthesis. *J. Am. Chem. Soc.* **136**, 9910–9913
8 Martin, J.L. and McMillan, F.M. (2002) SAM (dependent) I AM: the *S*-adenosylmethionine-dependent methyltransferase fold. *Curr. Opin. Struct. Biol.* **12**, 783–793
9 Studier, F.W. (2005) Protein production by auto-induction in high-density shaking cultures. *Protein Expr. Purif.* **41**, 207–234
10 Wang, Q.S., Yu, F., Huang, S., Sun, B., Zhang, K.H., Liu, K. et al. (2015) The macromolecular crystallography beamline of SSRF. *Nucl. Sci. Tech.* **26**, 010102
11 Vonrhein, C., Flensburg, C., Keller, P., Sharff, A., Smart, O., Paciorek, W. et al. (2011) Data processing and analysis with the *autoPROC* toolbox. *Acta Crystallogr. D Biol. Crystallogr.* **67**, 293–302
12 Kabsch, W. (2010) *Xds*. *Acta Crystallogr. D Biol. Crystallogr.* **66**, 125–132
13 Evans, P.R. and Murshudov, G.N. (2013) How good are my data and what is the resolution? *Acta Crystallogr. D Biol. Crystallogr.* **69**, 1204–1214
14 Fage, C.D., Isiorho, E.A., Liu, Y.N., Wagner, D.T., Liu, H.W. and Keatinge-Clay, A.T. (2015) The structure of spnF, a standalone enzyme that catalyzes [4+2] cycloaddition. *Nat. Chem. Biol.* **11**, 256–258
15 Adams, P.D., Afonine, P.V., Bunkóczi, G., Chen, V.B., Davis, I.W., Echols, N. et al. (2010) *PHENIX*: a comprehensive python-based system for macromolecular structure solution. *Acta Crystallogr. D Biol. Crystallogr.* **66**, 213–221

© 2016 The Author(s); published by Portland Press Limited on behalf of the Biochemical Society

16 Emsley, P., Lohkamp, B., Scott, W.G. and Cowtan, K. (2010) Features and development of *Coot*. *Acta Crystallogr. D Biol. Crystallogr.* **66**, 486–501
17 Chen, V.B., Arendall, W.B., Headd, J.J., Keedy, D.A., Immormino, R.M., Kapral, G.J. et al. (2010) *MolProbity*: all-atom structure validation for macromolecular crystallography. *Acta Crystallogr. D Biol. Crystallogr.* **66**, 12–21
18 Dolinsky, T.J., Nielsen, J.E., McCammon, J.A. and Baker, N.A. (2004) PDB2PQR: an automated pipeline for the setup of Poisson–Boltzmann electrostatics calculations. *Nucleic Acids Res.* **32**, W665–W667
19 Olsson, M.H.M., Søndergaard, C.R., Rostkowski, M. and Jensen, J.H. (2011) PROPKA3: consistent treatment of internal and surface residues in empirical pK_a predictions. *J. Chem. Theory Comput.* **7**, 525–537
20 Solórzano Kraemer, M.M., Kraemer, A.S., Stebner, F., Bickel, D.J. and Rust, J. (2015) Entrapment bias of arthropods in miocene amber revealed by trapping experiments in a tropical forest in Chiapas, Mexico. *PLoS One* **10**, e0118820
21 Schmidt, M.W., Baldridge, K.K., Boatz, J.A., Elbert, S.T., Gordon, M.S., Jensen, J.H. et al. (1993) General atomic and molecular electronic-Structure system. *J. Comput. Chem.* **14**, 1347–1363
22 Bayly, C.I., Cieplak, P., Cornell, W.D. and Kollman, P.A. (1993) A well-behaved electrostatic potential based method using charge restraints for deriving atomic charges: the RESP model. *J. Phys. Chem.* **97**, 10269–10280
23 Roe, D.R. and Cheatham, T.E. (2013) PTRAJ and CPPTRAJ: software for processing and analysis of molecular dynamics trajectory data. *J. Chem. Theory Comput.* **9**, 3084–3095
24 Patel, A., Chen, Z., Yang, Z., Gutiérrez, O., Liu, H.W., Houk, K.N. et al. (2016) Dynamically complex [6+4] and [4+2] cycloadditions in the biosynthesis of spinosyn A. *J. Am. Chem. Soc.* **138**, 3631–3634
25 Thoma, R., Schulz-Gasch, T., D'Arcy, B., Benz, J., Aebi, J., Dehmlow, H. et al. (2004) Insight into steroid scaffold formation from the structure of human oxidosqualene cyclase. *Nature* **432**, 118–122
26 Wendt, K.U., Poralla, K. and Schulz, G.E. (1997) Structure and function of a squalene cyclase. *Science* **277**, 1811–1815
27 Liscombe, D.K., Louie, G.V. and Noel, J.P. (2012) Architectures, mechanisms and molecular evolution of natural product methyltransferases. *Nat. Prod. Rep.* **29**, 1238–1250
28 Singh, S., Mccoy, J.G., Zhang, C., Bingman, C.A., Phillips, G.N. and Thorson, J.S. (2008) Structure and mechanism of the rebeccamycin sugar 4′-*O*-methyltransferase RebM. *J. Biol. Chem.* **283**, 22628–22636

© 2016 The Author(s); published by Portland Press Limited on behalf of the Biochemical Society